Support vector machine-based classification of neuroimages in Alzheimer's disease: direct comparison of FDG-PET, rCBF-SPECT and MRI data acquired from the same individuals

Journal:	*Revista Brasileira de Psiquiatria*
Manuscript ID	RBP-2016-OA-2083.R1
Manuscript Type:	Original Article
Date Submitted by the Author:	03-Apr-2017
Complete List of Authors:	Ferreira, Luiz; University of Sao Paulo, Psychiatry Rondina, Jane; University College London, London, United Kingdom, Department of Computer Science Kubo, Rodrigo; Faculty of Medicine, University of São Paulo, Department of Radiology and Oncology Ono, Carla; Faculty of Medicine, University of São Paulo, Department of Radiology and Oncology Leite, Claudia; Faculty of Medicine, University of São Paulo, Department of Radiology and Oncology Smid, Jerusa; Faculty of Medicine, University of São Paulo, Department of Neurology Bottino, Cássio; Faculty of Medicine, University of São Paulo, Department of Psychiatry Nitrini, Ricardo; Faculty of Medicine, University of São Paulo, Department of Neurology Filho, Geraldo; Faculty of Medicine, University of São Paulo, Department of Psychiatry Duran, Fabio; Faculty of Medicine, University of São Paulo, Department of Psychiatry Buchpiguel, Carlos; Faculty of Medicine, University of São Paulo, Department of Radiology and Oncology
Keywords:	Dementia - Alzheimer's Disease, Brain Imaging Techniques, Diagnosis And Classification, Memory, Neurology

Support vector machine-based classification of neuroimages in Alzheimer's disease: direct comparison of FDG-PET, rCBF-SPECT and MRI data acquired from the same individuals

Luiz Kobuti Ferreira[a,b]*, Jane Maryam Rondina[a,c], Rodrigo Kubo[d], Carla Rachel Ono[d,e], Claudia Costa Leite[f], Jerusa Smid[g], Cassio Bottino[h], Ricardo Nitrini[g], Geraldo F. Busatto[a,b,h], Fabio Luis de Souza Duran[a,b]‡, Carlos Alberto Buchpiguel[b,d,e]‡

[a]Laboratory of Psychiatric Neuroimaging (LIM 21), Department of Psychiatry, Faculty of Medicine, University of São Paulo, São Paulo, Brazil

[b]Center for Interdisciplinary Research on Applied Neurosciences (NAPNA), University of São Paulo, São Paulo, Brazil

[c]Sobell Department of Motor Neuroscience and Movement Disorders, Institute of Neurology, University College London, London, United Kingdom

[d]Nuclear Medicine Centre (LIM43), Department of Radiology and Oncology, Faculty of Medicine, University of São Paulo, São Paulo, Brazil

[e]Nuclear Medicine Division, Hospital do Coração da Associação Sanatório Sírio, São Paulo, Brazil.

[f]MRI Division, Department of Radiology and Oncology, Faculty of Medicine, University of São Paulo, São Paulo, Brazil

[g]Department of Neurology, Faculty of Medicine, University of São Paulo, São Paulo, Brazil

[h]Department of Psychiatry, Faculty of Medicine, University of São Paulo, São Paulo, Brazil

‡Co-senior authorship

*Corresponding author: Luiz Kobuti Ferreira: Email: kobuti.ferreira@gmail.com, Tel: +55 11 2661 8132. Address: Centro de Medicina Nuclear, 2o andar, LIM-21, Rua Dr. Ovídio Pires de Campos, s/n, Postal code CEP 05403-010, São Paulo, SP, Brazil.

Running title: SVM of PET, SPECT and MRI in Alzheimer's

ABSTRACT

Objective: To conduct the first support vector machine (SVM)-based study comparing the diagnostic accuracy of T1-weighted MRI (T1-MRI), FDG-PET and regional cerebral blood flow (rCBF) SPECT in Alzheimer's disease (AD).

Method: Brain T1-MRI, FDG-PET and rCBF-SPECT were acquired in exactly the same sample of mild AD patients (n=20) and elderly healthy controls (n=18). SVM-based diagnostic accuracy indices were calculated using whole-brain information and leave-one-out cross-validation approach.

Results: Accuracy obtained using PET and SPECT data were similar (PET accuracy was 68~71% and AUC 0.77~0.81; SPECT accuracy was 68~74% and AUC 0.75~0.79), and both had better performance relative to the analysis using T1-MRI data (accuracy of 58%, AUC 0.67). The addition of PET or SPECT to MRI produced higher accuracy indices (68~74%; AUC: 0.74~0.82) than T1-MRI alone but these were not clearly superior to the isolated neurofunctional modalities.

Conclusion: In line with previous evidence, FDG-PET and rCBF-SPECT more accurately identified patients with AD than T1-MRI and the addition of either PET or SPECT to T1-MRI data yielded increased accuracy. The comparable SPECT and PET performances, directly demonstrated for the first time in the present study, support the view that rCBF-SPECT still has a role to play in the diagnosis of AD.

Keywords: Alzheimer's disease; support vector machine; MRI; FDG-PET; SPECT

1. Introduction

Alzheimer's disease (AD) is characterized by structural and metabolic changes in the brain. The most consistent evidence of AD-related neuronal degeneration includes grey matter atrophy in the temporal lobes and medial parietal cortex and hypometabolism in the temporoparietal cortex.[1,2]

The diagnosis of AD is mainly based on the detection of characteristic patterns of cognitive decline. The onset of AD is typically insidious – cognitive decline generally begins years before reaching threshold of clinical significance and causing functional impairment. Neuropsychological testing can help to identify and quantify such cognitive deficits, thus improving diagnostic certainty. Exclusion of other diseases is also a fundamental part of the diagnostic process and this requires blood tests and neuroimaging investigations. [1,2]

T1-weighted magnetic resonance imaging (MRI) is widely used both to rule out non-AD pathological processes (such as brain tumors and infarcts) and to characterize a typical AD-related pattern of atrophy in the temporal lobe and medial parietal cortex. Functional neuroimaging modalities, including ^{18}F-fluorodeoxyglucose-positron emission tomography (FDG-PET) and regional cerebral blood flow single photon emission computed tomography (rCBF-SPECT) frequently show a typical pattern of hypometabolism/hypoperfusion in temporoparietal regions and can be useful in cases of diagnostic uncertainty. While FDG-PET has greater sensitivity and specificity to detect AD-related hypofunctional brain patterns, the rCBF SPECT method is more readily available and less expensive in clinical settings.[3,4] These functional modalities should not be used as the only imaging measures during the diagnostic workup because they cannot provide necessary structural data to exclude non-AD diagnoses causing cognitive decline.[1,2] Although studies of samples of AD patients using mean

neuroimaging indices have brought major advances in the characterization of group-wise brain abnormalities,[5,6] the diagnosis of single individuals based solely on neuroimaging data is still not possible and brain findings can vary greatly between patients.

Diagnosis of early AD can be challenging. The task of summarizing the complex, highly dimensional neuroimaging data into a single label - the presence or absence of disease - has been addressed with the use of machine learning-based pattern recognition techniques in different neuropsychiatric disorders.[7] Support vector machine (SVM) is a multivariate machine learning approach that aims at classifying individuals using pattern recognition analysis. The aim of SVM is to find the best hyperplane that separates all data points of one group from those of another group.[8,9] SVM can potentially be applied to multimodal neuroimaging data in order to improve the accuracy of AD diagnosis.[10,11]

Both FDG-PET and rCBF-SPECT can be combined with neurostructural data to provide complementary information about brain changes associated with AD.[1] A recent systematic review found that although FDG-PET can be more accurate to distinguish among different types of dementia, it is only marginally superior or even equal to rCBF-SPECT to differentiate AD patients from healthy controls.[12] Nevertheless, evidence from studies comparing rCBF-SPECT and FDG-PET is still "limited and inadequate" and none of the studies included in that review performed SVM analyses.[12]

SVM has been used in studies of AD investigating combinations of T1-MRI + FDG-PET[13-16] but we are not aware of any SVM study investigating SVM performance to discriminate AD from controls using a combination of T1-MRI, FDG-PET and rCBF-SPECT acquired in the

same sample. Therefore, it is still unknown whether a combination of T1-MRI plus FDG-PET is superior to T1-MRI plus rCBF-SPECT.

Intensity normalization is a standard step in studies using FDG-PET and SPECT, either using the total tracer uptake in the brain or the uptake in a single reference brain region. This procedure minimizes the effects of inter-individual differences in absolute whole brain signal, allowing the identification of regional patterns of change in metabolic activity.[17,18] The cerebellum is often used as reference because it is known to be spared in AD[13,18] but both cerebellar and global uptake normalization have been used in SVM studies of AD.[13,19] Based on the idea that the region of reference should be unaffected by the investigated disease[18] and on previous semi-quantitative FDG-PET and rCBF-SPECT studies that compared AD and controls,[17,20] one would expect that cerebellar normalization could improve diagnostic accuracy. However, no SVM study to date directly compared the diagnostic accuracy of cerebellar and global normalization when distinguishing AD from controls.

The aim of the present study is to evaluate the diagnostic accuracy of SVM to distinguish patients with AD from healthy controls using neurostructural (T1-MRI) and neurofunctional imaging data (both FDG-PET and rCBF-SPECT). We wished to measure performance using the neuroimaging data (both in isolation and in combination) and characterize the optimal combination of imaging modalities. Moreover, we aimed to test if normalizing the radiotracer uptake to the cerebellum (for PET and SPECT data) would improve the diagnostic performance of the classifier.

2. Methods

2.1.Study population

Twenty patients with mild AD and a group of 18 controls comprised by healthy elderly volunteers were enrolled. The ethical committee of the institutions involved in the study approved the investigation. Informed consent was obtained from all participants.

Patients were recruited by the time of their first visit at memory outpatient clinics of the departments of Neurology and Psychiatry of the University of São Paulo Medical School. All patients fulfilled the DSM-III-R[21] criteria for mild dementia and NINCDS/ADRDA[22] criteria for probable AD. The Clinical Dementia Rating (CDR) scale[23] was used to assess clinical severity and only patients with CDR equal to 0.5 or 1 (i.e. mild dementia) were included. Patients with auditory deficits or uncorrected visual impairments that could interfere with their cognitive evaluation were excluded. Patients should not have been under pharmacological treatment for AD with cholinesterase inhibitors.

Exclusion criteria for both the AD and control groups were: less than four years of education, age below 60 or above 90 years, use of psychotropic drugs, diabetes mellitus, presence of systemic disorders associated with cognitive impairment and brain lesions incidentally detected on MRI. Family history of AD as well as information about current and previous medical, neurological and psychiatric illness was obtained during the interview with the participants and their families. History of neurologic or psychiatric disorders prior to the onset of AD and presence of diabetes mellitus and severe medical conditions were also exclusion criteria.

Patients with AD underwent an extensive neuropsychological assessment including the following tests: The Mattis Dementia Rating Scale (DRS),[24] Trail-making test parts A and B, Hopper Visual Organization Test, Rey Auditory Verbal Learning Test, Wechsler Memory

Scale: logic memory and visual reproduction subtests, The Rey–Osterrieth complex figure test, Boston Naming Test and the Wisconsin Card Sorting Test. Instrumental activities of daily living were quantified with The Functional Activities Questionnaire.[25]

The AD group (11 female) had a mean age of 75.5 ± 4.0 years and their mean educational level was 7.3 ± 3.9 years. Mean Mini–Mental State Examination (MMSE) score was 21.3 ± 2.3, and the mean time course of AD was 22.5 ± 11.0 months. All patients presented a typical slow and gradual onset of symptoms, with onset of clinically relevant cognitive changes dating in average 22.5±11 months before enrolment for the study. The average of AD group's global functioning as assessed with The Functional Activities Questionnaire[25] was 10± 6.2 points. All AD patients were right-handed. Five patients had a family history of dementia, but without a dominant pattern of inheritance.

Healthy controls were recruited from activity centres and groups for elderly individuals in the community (11 female, mean age of 72.7 ±4.2 years, average years of education equal to 10.4 ± 4.8). They did not present memory complaints, their physical and neurological examination was normal and their score on the CDR scale was 0 (no deficit). They underwent a comprehensive neuropsychological evaluation (including MMSE) to objectively rule out cognitive deficits[26] and a self-reporting questionnaire[27] was used to exclude depression and other mental disorders (all individuals had scores lower than 8). All controls except one were right-handed. Volunteers with a family history of AD or any other form of dementia were excluded.

The demographic characteristics of the two groups are presented in Table 1. There was a trend towards greater age and lesser years of formal education in the AD sample compared to

controls. Further details about the enrolment requirements and the sample characteristics have been described in Buchpiguel et al., 2014.[28]

Table 1. Demographic characteristics of the sample.

	Normal participants	Patients with AD	*p*-value*
Age: mean (standard deviation)	72.7 (4.2)	75.5 (4.0)	0.06
Sex, number of participants: Male (Female)	7 (11)	9 (11)	0.70
Education, years: mean (standard deviation)	10.4 (4.8)	7.3 (3.9)	0.05
MMSE: mean (standard deviation)	28.1 (1.3)	21.3 (2.8)	< 0.01

AD, Alzheimer's disease. *p-value for Mann-Whitney tests (continuous variables) or chi-square test (gender)

2.2.Image Acquisition

2.2.1.Magnetic Resonance Imaging (MRI)

Spin echo T1-weighted images were obtained using a General Electric-Horizon LX 8.3 1.5 Tesla scanner (Milwaukee, WI, USA) on the sagittal plane with the following parameters: TR 12.1, TE 4.1999, flip angle 15^{o}, pixel bandwidth 88.75, matrix 256x256, voxel size 0.86x0.86x1.6mm, 204 slices, slice thickness 1.6.

2.2.2.Positron Emission Tomography (PET)

All subjects had blood glucose levels determined, according to a standard protocol. After at least a 6-hour fasting period, 370 MBq of [18F] fluor-2-D-deoxyglucose (FDG) was administered. The scans were performed on a dedicated LSO-PET 16-slice CT scanner (Biograph-16, Siemens, Illinois-USA). Imaging started 60 minutes after FDG administration, using a 3-D protocol with an acquisition time of 15 minutes. The matrix size was 256 x 256 with a smoothing factor of 5. Iterative reconstruction (OSEM) was applied according to a standardized protocol in our institution. Attenuation correction was done using the CT-algorithm.

2.2.3.Single Photon Emission Computed Tomography (SPECT)

Acquisition was started 30 minutes after IV injection of 20 mCi (740 MBq) of ^{99m}Tc-ECD and was obtained with a dual-detector SPECT camera equipped with a fan beam collimator (ECAM, Siemens, Hoffmann Estates, Illinois). Images were processed using a standard protocol, with no attenuation correction and a Butterworth post filtering. The reconstruction yielded 4.8 mm voxels with a 128 x 128 matrix and 128 slices. In-plane spatial resolution was 10.6 / 6.7 mm full width at a half maximum (FWHM) in the centre of view. Images were reconstructed with scatter correction.

2.3.Image Preprocessing

Initially, the images were converted from DICOM format to ANALYSE format using (X) Medcon software, version 0.8.12 (http://xmedcon.sourceforge.net). The origin of all images was set at the anterior commissure.

2.3.1.MRI preprocessing

We removed non-brain tissues (skull stripping) from the T1-MRI anatomical images as follows: firstly, we applied the Hybrid Watershed algorithm[29] (Freesurfer v.3.04, http://surfer.nmr.mgh.harvard.edu). Experienced technicians visually inspected the output and, if necessary, manual editing was performed using Freesurfer. Then, we performed intensity normalization using the N3 algorithm (Freesurfer).[30] As a final step, we used the Brain Extraction Tool[31] (FSL, www.fmrib.ox.ac.uk/fsl).

The images were segmented into grey matter (GM) and white matter partitions using the unified segmentation procedure described by Ashburner and Friston[32] (SPM8, http://www.fil.ion.ucl.ac.uk/spm), executed in Matlab R2012a (MathWorks Inc., Sherborn, MA, USA). The Diffeomorphic Anatomical Registration Through Exponentiated Lie Algebra (DARTEL) algorithm[33] was used to spatially normalize the segmented images to the standard MNI space. These normalized images were resliced with trilinear interpolation to a final voxel size of 2x2x2mm³. An additional "modulation" step consisted of multiplying each spatially normalized GM image by its relative volume before and after normalization, ensuring that the total amount of GM in each voxel was preserved. Finally, the resulting GM images were smoothed using an 8mm isotropic kernel at full width half maximum (FWHM).

2.3.2.FDG-PET and rCBF-SPECT preprocessing

FDG-PET and rCBF-SPECT images were coregistered to the skull striped T1-MRIin its native space using SPM8. Then, we performed partial volume effects (PVE) correction to avoid confounding effects related to regional brain atrophy.[34] We applied the Meltzer method, a voxel-based PVE correction algorithm (PVElab, http://nru.dk/downloads/software).[35,36] Because the Meltzer PVE correction method has been well validated for FDG-PET but not for SPECT images, the latter were preprocessed both with and without PVE correction (all SPECT-related analyses were performed twice: with and without PVE correction).

The spatial transformation resulting from the T1-MRI normalization steps (see above) were applied to the FDG-PET and SPECT images in order to achieve spatial normalization to the standard MNI space. The normalized images were smoothed with a Gaussian filter of 8mm at FWHM.

We implemented two independent approaches for PET and SPECT intensity normalization. Global normalization was achieved by dividing the value of each voxel by the average of all voxels belonging to a whole brain mask. As an alternative to global normalization, we performed cerebellar normalization by dividing the value of each voxel by the average of the voxels belonging to a region of interest comprising the superior portion of the cerebellum and the vermis - regions cerebellum III, IV, V, VI and the entire vermis from the AAL atlas,[37] as previously described.[20] We ran separate analyses using images with global and cerebellar normalization in order to compare these two approaches.

2.4.Classification using Support Vector Machine

We employed a whole-brain approach using a mask to exclude voxels outside the brain. This resulted in feature vectors with 219727 voxels for all modalities (each feature corresponds to a brain voxel).

We applied SVM[8,9,38,39] implemented in the library libsvm[40] available in the toolbox PRoNTo[11] to classify controls (class 1) and AD patients (class 2). Considering that the number of features is very large, we used a linear kernel, as there is no need to map them to an even higher dimensional feature space to separate the examples. Due to the comparative nature of our investigation, the soft-margin SVM penalty parameter *C* was fixed to 1, so no grid search was performed to find the optimal parameter when classifying.

As the AD sample presented trends towards being older and having less years of education than controls (Table 1), the neuroimaging data was corrected for the effects of age and education. This was performed by linear algebra operations involving matrix transformation to remove confounding effects on the kernels using a residual form matrix.[41,42]

During the training phase, the SVM algorithm finds a hyperplane that separates the examples in the input space maximizing the margin of separation between the classes. Support vectors are data points that lie closest to the separating hyperplane. Once the decision function is determined from the training data, it can be used to predict the class label of a new test example.[43]

To evaluate the generalization ability of the model, the dataset was partitioned into a 'training set' and a 'testing set'. By repeatedly repartitioning the data in this way we obtained an estimate of the generalization error of the model. We used a 'Leave–one–out' cross validation

approach,[44,45] where one single example (corresponding to either a patient or a healthy control) was left out for testing in each iteration.

The accuracy was obtained through the number of true positives (patients correctly classified) and true negatives (healthy controls correctly classified). As the number of examples in each class is different, we calculated a measure of balanced accuracy, which takes the number of samples in each class into account, giving equal weight to the accuracies obtained on test samples. Additionally, we compared the different models using ROC (receiver operating characteristic) curves, plotting the true positive rate against the false positive rating along different threshold values. The area under the curve (AUC) is a summary measure describing the performance of the classifier across all decision thresholds.

Statistical significance was tested using permutations, a non-parametric approach by which the frequency distribution under the null hypothesis is obtained by calculating many possible combinations under rearrangements of the labels (i.e. 'patients' vs. 'controls') across the examples. We randomly exchanged the labels associated to the examples and repeated the complete procedure (leave-one-out training and test) 1000 times. As the correlation between examples and labels is destroyed, one expects the classification accuracy with permuted labels to be close to chance (around 50%). Figure 1 describes schematically the flow chart of the SVM analysis.

Figure 1. Flow chart of SVM analysis.

[Fig1_SVM_Flowchart.tif]

AD: Alzheimer's disease; AUC, area under curve; BA: balanced accuracy; FDG-PET: ^{18}F-fluorodeoxyglucose-positron emission tomography; SPECT: single photon emission computed

tomography; SVM: support vector machine; T1-MRI: T1-weighted magnetic resonance imaging; TN: true negative TP: true positive.

3. Results

3.1.Single-modality

Table 2 presents the results of analyses performed for each modality individually and Figure 2 presents the ROC curve for each of the functional imaging modalities compared with the T1-MRI data. The best accuracy to distinguish AD from controls was obtained using neurofunctional data. Classification using rCBF-SPECT resulted in an AUC of 0.75~0.79 and an accuracy of 68~74% and FDG-PET data resulted in an AUC of 0.77~0.81, with accuracy of 68~71%. T1-MRI was the modality presenting the worse performance, with 58% accuracy and an AUC of 0.67. Classification accuracy using neurofunctional data reached statistically significant values while this did not happen when using only MRI (Table 2). The different preprocessing pipelines for the neurofunctional data did not yield clear differences in diagnostic performance.

Figure 2. Receiver operating characteristic (ROC) curves of single modality classification.

[Fig2_ROC_Single_Modalities.tif]

CN: cerebellar normalization; FDG-PET: ^{18}F-fluorodeoxyglucose-positron emission tomography; GN: global normalization; PVE: partial volume effect correction; SPECT: single photon emission computed tomography; T1-MRI: T1-weighted magnetic resonance imaging.

Table 2. Classification accuracy for each image modality

Modality			AUC	TP	TN	BA	*p*
T1-MRI			0.67	50.00%	66.67%	58.33%	0.1379
FDG-PET	GN		0.81	70.00%	66.67%	68.33%	0.0242
	CN		0.77	70.00%	72.22%	71.11%	0.0157
rCBF-SPECT	GN	PVE	0.75	60.00%	77.78%	68.89%	0.0210
		No PVE	0.76	70.00%	66.67%	68.33%	0.0214
	CN	PVE	0.75	60.00%	83.33%	71.67%	0.0071
		No PVE	0.79	70.00%	77.78%	73.89%	0.0043

AUC, area under curve; BA: balanced accuracy; CN: cerebellar normalization; FDG-PET: ^{18}F-fluorodeoxyglucose-positron emission tomography; GN: global normalization; *p*: Non-parametric statistical significance; PVE: partial volume effect correction; rCBF-SPECT: regional cerebral blood flow single photon emission computed tomography; T1-MRI: T1-weighted magnetic resonance imaging; TN: true negative TP: true positive.

Figure 3 shows a graphical representation of predictions for each single-modality classification (T1-MRI, FDG-PET and rCBF-SPECT). As multiple analyses were performed for FDG-PET and rCBF-SPECT, this figure presents only the classifications that resulted in the best accuracies for each modality (i.e. rCBF-SPECT without correction for PVE and both FDG-PET and rCBF-SPECT with cerebellar normalization). Subjects classified as healthy controls are plotted to the left of the dotted vertical line (i.e. with negative SVM projections) while subjects to the right of the vertical line presented positive SVM projections and were thus classified as having AD. Classification using only T1-MRI data resulted in more incorrect labeling than when using either only FDG-PET or only rCBF-SPECT.

Figure 3. SVM class prediction of individual subjects for each imaging modality.

[Fig3_Individual_Predictions.tif]

Y-axis: subject's identification number. X-axis: linear projection of each subject. Subjects receiving negative values (i.e. data points to the left of the vertical dotted line) were classified as Controls while those receiving positive values (i.e. to the right of the vertical line) were classified as having Alzheimer's disease (AD). Misclassifications can be observed as circles at the left side of the separating plane (AD patients incorrectly classified as Controls, i.e. false negatives) and crosses at the right side of it (Controls incorrectly classified as AD patients, i.e. false positives).
FDG-PET: ^{18}F-fluorodeoxyglucose-positron emission tomography; SPECT: single photon emission computed tomography; SVM, support vector machine; T1-MRI: T1-weighted magnetic resonance imaging.

Figure 4 presents the three discriminant maps showing the relative weight of brain voxels resulting from the application of linear SVM to classify AD patients *versus* controls using each imaging modality (T1-MRI, FDG-PET and rCBF-SPECT). We can observe in Figure 4 that the classifications based on the three different modalities produce different global patterns of anatomical distribution of voxel weights.

Figure 4. Patterns of anatomical distribution of voxel weights resulting from single-modality classifications.

[Fig4_WeightMaps.tif]

Positive weights mean a higher relative measure in that voxel for AD patients compared to Controls. Conversely, a negative weight means a higher relative measure for Controls. The measures are: grey matter volume for T1-MRI, regional brain metabolism for FDG-PET and regional cerebral blood flow for rCBF-SPECT.
CN: cerebellar normalization; FDG-PET: ^{18}F-fluorodeoxyglucose-positron emission tomography; GN: global normalization; PVE: partial volume effect correction; SPECT: single photon emission computed tomography; T1-MRI: T1-weighted magnetic resonance imaging.

3.2.Combining Modalities

The combination of neurofunctional data (FDG-PET or rCBF-SPECT) to T1-MRI yielded better classification accuracies (68~74% vs. 58%) and improved AUC (0.74~0.82 vs. 0.67) than the neuroanatomical data. However, the combination of modalities did not present a clear improvement when compared to isolated neurofunctional data. Table 3 presents the results of analyses with combination of modalities and Figure 5 the ROC curves of each combination of modalities.

Table 3. Classification accuracy for the combination of image modalities

	AUC	TP	TN	BA	*p*
T1-MRI + FDG-PET (GN)	0.81	75.00%	66.67%	70.83%	0.0198
T1-MRI + FDG-PET (CN)	0.82	70.00%	72.22%	71.11%	0.0014
T1-MRI + rCBF-SPECT (GN; PVE)	0.78	75.00%	72.22%	73.61%	0.0008
T1-MRI + rCBF-SPECT (CN; PVE)	0.74	70.00%	66.67%	68.33%	0.0253
T1-MRI + rCBF-SPECT (GN; No PVE)	0.78	80.00%	66.67%	73.33%	0.0011
T1-MRI + rCBF-SPECT (CN; No PVE)	0.76	75.00%	72.22%	73.61%	0.0003

AUC, area under curve; BA: balanced accuracy; CN: cerebellar normalization; FDG-PET: ^{18}F-fluorodeoxyglucose-positron emission tomography; GN: global normalization; *p*: Non-parametric statistical significance; PVE: partial volume effect correction; rCBF-SPECT: regional cerebral blood flow single photon emission computed tomography; T1-MRI: T1-weighted magnetic resonance imaging; TN: true negative; TP: true positive.

Figure 5. Receiver operating characteristic (ROC) curves of classifications using combination of imaging modalities.

[Fig5_ROC_Combined_Modalities.tif]

CN: cerebellar normalization; FDG-PET: ^{18}F-fluorodeoxyglucose-positron emission tomography; GN: global normalization; PVE: partial volume effect correction; SPECT: single photon emission computed tomography; T1-MRI: T1-weighted magnetic resonance imaging.

4. Discussion

To the best of our knowledge, this is the first SVM-based neuroimaging study that conducted comparative diagnostic accuracy assessments of brain T1-MRI, FDG-PET and rCBF-SPECT data acquired from exactly the same AD patients and controls.

The lowest diagnostic accuracy was the one based solely on T1-MRI data. One possibility is that nonspecific findings of brain atrophy - variably detected in cognitively preserved elderly subjects - may complicate the discrimination when SVM methods are applied. Also, in SVM investigations with samples of modest size (as in our case), variations in a single MRI dataset (for instance due to movement during scanning) may more significantly affect diagnostic performance.[46] The higher accuracy indices of neurofunctional data relative to MRI-based data is in accordance with previous T1-MRI and FDG-PET studies,[13,14] confirming the notion that brain metabolic markers more accurately differentiate AD-related pathological changes from the effects of healthy aging on the brain.[14] Moreover, multimodal neuroimaging studies have suggested that metabolic changes precede atrophy in AD.[47] In accordance to this, the use of imaging modalities sensitive to hypometabolism, such as FDG-PET and rCBF-SPECT, resulted in better accuracies than classification using T1-MRI, especially considering that the sample consisted of patients with mild dementia.

Previous studies have used a number of different classification techniques with variable results[48-51] but, to our knowledge, our study is the first to indicate directly that a multivariate analysis resulted in rCBF-SPECT accuracy indices comparable to FDG-PET. Our rCBF-SPECT findings concur with the results of other SPECT studies of AD.[52,53] Thus, this imaging technique may still have a role in assisting the diagnosis of AD, especially given its wider availability in some environments as compared to FDG-PET.

In the present study, combining neurofunctional to neuroanatomical data yielded higher accuracy indices than when using only T1-MRI images and this is in line with previous investigations.[13,14] Although adding neurofunctional data to neuroanatomical data yielded better results, the accuracy resulting from the combination of modalities was not clearly superior to the accuracy of isolated neurofunctional modalities, which is also in accordance with previous PET and MRI studies.[13,14] This may be due to the whole brain approach because others have shown that using data extracted only from disease-related regions of interest can result in increased classification accuracy of MRI-T1+FDG-PET when compared to single modality FDG-PET.[13,54]

Previous SVM-based investigations using FDG-PET or rCBF-SPECT data did not compare the diagnostic accuracy of cerebellar *versus* global normalization to distinguish AD from controls. In this study the accuracy indices were similar with the two tracer normalization procedures. This suggests that although the normalization procedure can yield different results in studies comparing mean functional data between groups of healthy controls and AD,[55] the normalization approach is not as critical when classifying individuals using pattern recognition analysis.

There are a number of strengths in the present study that should be highlighted, such as the careful selection and clinical assessment of controls and patients in early AD stages. All three images modalities were performed in all subjects, allowing for direct comparison of the classifier performance between modalities and combination of modalities. Moreover, we employed state-of-the-art methods to correct functional neuroimaging data for PVE.

The relatively modest size of the samples is an important limitation of the study, and this probably influenced on the lower accuracy figures reported in our study as compared to studies with larger samples,[46] particularly in regard to the T1-based MRI data. However, the novelty of our study lies not in the reporting of how well neuroimaging-based diagnostic performance indices can discriminate AD from controls using SVM, but rather on the direct head-to-head comparisons across neuroimaging modalities, particularly taking advantage of the acquisition of both PET and SPECT data in exactly the same AD patients and controls. Indeed, the SVM-based evaluation of such modestly sized but carefully screened sample has still provided sufficient power to produce high diagnostic accuracy scores when either of such neurofunctional modalities was included in the analyses. One other limitation of our study is that we did not use any scale to document the presence and severity of neuropsychiatric symptoms, which are very common in AD.[56] The lack of this information is a common limitation in the field, shared also by other studies of SVM in AD.[13-16] It is important to stress that neurologic or psychiatric disorders prior to the onset of AD were exclusion criteria and that the development of neuropsychiatric symptoms has been considered a core feature of AD.[56] Therefore we believe that in our study there would be no need to correct the data for the presence of these symptoms. A third limitation worth mentioning is that T1-MRI data was acquired using a 1.5 Tesla scanner and it is possible that higher accuracies would emerge if a 3T scanner had been used. Finally, although the SVM analysis conducted herein allowed testing the accuracy of the machine learning-based approach with no need to define anatomical hypotheses *a priori,* this whole-brain multivariate approach limits the interpretability of brain anatomical results. Therefore, although the attribution of voxel weights was available, we refrain from drawing any conclusions about the involvement of specific brain regions. We are currently aiming at addressing this issue in additional investigations using our multimodal

imaging data, using an approach more suited to extract anatomical information from SVM analyses.[57]

The number of studies using machine learning approaches to deal with the large amount of data generated by neuroimaging investigations is growing fast, and future studies are expected to bring new insights and possibilities. For instance, the application of SVM techniques to neurofunctional and neurostructural data has already shown the potential to predict future cognitive decline and conversion from mild cognitive impairment to AD.[58] Another idea is to use longitudinal neuroimaging data (i.e. rate of change) as input to the classifier.[59,60] One additional alternative is to apply a probabilistic framework that allows the determination of likelihood of diagnosis so that the concept of disease as a spectrum from normality to overt AD can be reflected on the analytical approach.[61] Another interesting idea is to apply machine-learning techniques to combine neuroimaging data with other types of biomarkers (e.g. CSF Aβ42, t-tau and p-tau; APOE genotype) to further improve accuracy.[61,62] Finally, it is worth mentioning that SVM is a popular multivariate machine learning approach but there are also other methods of such kind that have been applied to neuroimaging studies of AD, such as Naive Bayes, Gaussian process and neural network classifications.[61,63-65]

Concluding, SVM performance using neurofunctional data (FDG-PET and rCBF-SPECT) was superior to performance using T1-MRI to distinguish AD from controls. The combination of neurofunctional and volumetric data yielded higher accuracies than isolated T1-MR. Classification using SPECT presented similar results to those obtained with FDG-PET.

Acknowledgments

This study was supported by São Paulo Research Foundation (Fundação de Amparo à Pesquisa do Estado de São Paulo - FAPESP, grants 2004/05551-6 and 2012/50329-6).

Disclosure

Carlos A. Buchpiguel was supported by São Paulo Research Foundation (Fundação de Amparo à Pesquisa do Estado de São Paulo – FAPESP, grant 2004/05551-6).

Jane Maryam Rondina was supported by "Efficacy and Mechanism Evaluation (EME) Programme" Medical Research Council (MRC) and National Institute for Health Research (NIHR, United Kingdom) partnership.

Geraldo F. Busatto was supported by Conselho Nacional de Desenvolvimento Científico e Tecnológico (CNPq, Brazil) and by São Paulo Research Foundation (Fundação de Amparo à Pesquisa do Estado de São Paulo – FAPESP, grant 2012/50329-6).

References

1. Ferreira LK, Busatto GF. Neuroimaging in Alzheimer's disease: current role in clinical practice and potential future applications. Clinics 2011;66:19–24.

2. McKhann GM, Knopman DS, Chertkow H, Hyman BT, Jack CR Jr., Kawas CH, et al. The diagnosis of dementia due to Alzheimer's disease: Recommendations from the National Institute on Aging-Alzheimer's Association workgroups on diagnostic guidelines for Alzheimer's disease. Alzheimers Dement 2011;7:263–9.

3. Brooks DJ. Positron emission tomography and single-photon emission computed tomography in central nervous system drug development. NeuroRx 2005;2:226–36.

4. Matsuda H. Role of neuroimaging in Alzheimer's disease, with emphasis on brain perfusion SPECT. J Nucl Med 2007;48:1289–300.

5. Busatto GF, Diniz BS, Zanetti MV. Voxel-based morphometry in Alzheimer's disease. Expert Rev Neurotherapeutics 2008;8:1691–702.

6. Frisoni GB, Pievani M, Testa C, Sabattoli F, Bresciani L, Bonetti M, et al. The topography of grey matter involvement in early and late onset Alzheimer's disease. Brain 2007;130:720–30.

7. Orrù G, Pettersson-Yeo W, Marquand AF, Sartori G, Mechelli A. Using Support Vector Machine to identify imaging biomarkers of neurological and psychiatric disease: A critical review. Neurosci Biobehav R 2012;36:1140–52.

8. Boser BE, Guyon IM, Vapnik VN. A training algorithm for margin optimal classifiers. Proceedings of the fifth annual workshop on computational learning theory 1992;1:144–52.

9. Cortes C, Vapnik V. Support-Vector Networks. Mach Learn 1995;20:273–97.

10. Dyrba M, Ewers M, Wegrzyn M, Kilimann I, Plant C, Oswald A, et al. Combining DTI and MRI for the Automated Detection of Alzheimer's Disease Using a Large European Multicenter Dataset. In: Yap P-T, Liu T, Shen D, Westin C-F, Shen L, editors. Multimodal Brain Image Analysis. Berlin: Springer Berlin Heidelberg; 2012. pages 18–28.

11. Schrouff J, Rosa MJ, Rondina JM, Marquand AF, Chu C, Ashburner J, et al. PRoNTo: Pattern Recognition for Neuroimaging Toolbox. Neuroinformatics 2013;11:319–37.

12. Davison CM, O'Brien JT. A comparison of FDG-PET and blood flow SPECT in the diagnosis of neurodegenerative dementias: a systematic review. Int J Geriatr Psych 2014;29:551–61.

13. Dukart J, Mueller K, Horstmann A, Barthel H, Möller HE, Villringer A, et al. Combined Evaluation of FDG-PET and MRI Improves Detection and Differentiation of Dementia. PLoS ONE 2011;6:e18111.

14. Dukart J, Mueller K, Barthel H, Villringer A, Sabri O, Schroeter ML, et al. Meta-analysis based SVM classification enables accurate detection of Alzheimer's disease across different clinical centers using FDG-PET and MRI. Psychiat Res-Neuroim 2013;212:230–6.

15. Jie B, Zhang D, Cheng B, Shen D, Alzheimer's Disease Neuroimaging Initiative. Manifold regularized multitask feature learning for multimodality disease classification. Hum Brain Mapp 2015;36:489–507.

16. Liu F, Wee C-Y, Chen H, Shen D. Inter-modality relationship constrained multi-modality multi-task feature selection for Alzheimer's Disease and mild cognitive impairment identification. Neuroimage 2014;84:466–75.

17. Dukart J, Mueller K, Horstmann A, Vogt B, Frisch S, Barthel H, et al. Differential effects of global and cerebellar normalization on detection and differentiation of dementia in FDG-PET studies. Neuroimage 2010;49:1490–5.

18. Yakushev I, Landvogt C, Buchholz H-G, Fellgiebel A, Hammers A, Scheurich A, et al. Choice of reference area in studies of Alzheimer's disease using positron emission tomography with fluorodeoxyglucose-F18. Psychiat Res-Neuroim 2008;164:143–53.

19. Horn J-F, Habert M-O, Kas A, Malek Z, Maksud P, Lacomblez L, et al. Differential automatic diagnosis between Alzheimer's disease and frontotemporal dementia based on perfusion SPECT images. Artif Intell Med 2009;47:147–58.

20. Rasmussen JM, Lakatos A, van Erp TGM, Kruggel F, Keator DB, Fallon JT, et al. Empirical derivation of the reference region for computing diagnostic sensitive [1]□fluorodeoxyglucose ratios in Alzheimer's disease based on the ADNI sample. Biochim Biophys Acta 2012;1822:457–66.

21. American Psychiatric Association. Diagnostic and statistical manual of mental disorders (DSM–III–R). 3rd ed. Washington, DC: American Psychiatric In; 1987.

22. McKhann GM, DrachMAN D, Folstein MF, Katzman R, Price D, Stadlan EM. Clinical diagnosis of Alzheimer"s disease: report of the NINCDS-ADRDA Work Group under the auspices of Department of Health and Human Services Task Force on Alzheimer"s Disease. Neurology 1984;34:939–44.

23. Morris JC. The Clinical Dementia Rating (CDR): current version and scoring rules. Neurology 1993;43:2412–4.

24. Mattis S. Dementia Rating Scale - Professional Manual. Florida: Psychological Assessment Resources; 1988.

25. Pfeffer RI, Kurosaki TT, Harrah CH, Chance JM, Filos S. Measurement of functional activities in older adults in the community. J Gerontol 1982;37:323–9.

26. Nitrini R, Caramelli P, Porto CS, H C-F, AP F, Carthery-Goulart MT, et al. Brief cognitive battery in the diagnosis of mild Alzheimer's disease in subjects with medium and high levels of education. Dement Neuropsychol 2007;1:32–6.

27. Harding TW, de Arango MV, Baltazar J, Climent CE, Ibrahim HH, Ladrido-Ignacio L, et al. Mental disorders in primary health care: a study of their frequency and diagnosis in four developing countries. Psychol Med 1980;10:231–41.

28. Buchpiguel CA, Smid J, Duran FL, Bottino C, Ono CR, Leite CC, et al. Brain MRI, SPECT and PET in early Alzheimer's disease: a minor mismatch between volumetric and functional findings. Curr Mol Imaging 2014;3:1–9.

29. Ségonne F, Dale AM, Busa E, Glessner M, Salat D, Hahn HK, et al. A hybrid approach to the skull stripping problem in MRI. Neuroimage 2004;22:1060–75.

30. Sled JG, Zijdenbos AP, Evans AC. A nonparametric method for automatic correction of intensity nonuniformity in MRI data. IEEE T Med Imaging 1998;17:87–97.

31. Smith SM. Fast robust automated brain extraction. Hum Brain Mapp 2002;17:143–55.

32. Ashburner J, Friston KJ. Unified segmentation. Neuroimage 2005;26:839–51.

33. Ashburner J. A fast diffeomorphic image registration algorithm. Neuroimage 2007;38:95–113.

34. Curiati PK, Tamashiro-Duran JH, Duran FLS, Buchpiguel CA, Squarzoni P, Romano DC, et al. Age-related metabolic profiles in cognitively healthy elders: results from a voxel-based [18F]fluorodeoxyglucose-positron-emission tomography study with partial volume effects correction. Am J Neuroradiol 2011;32:560–5.

35. Meltzer CC, Cantwell MN, Greer PJ, Ben-Eliezer D, Smith G, Frank G, et al. Does cerebral blood flow decline in healthy aging? A PET study with partial-volume correction. J Nucl Med 2000;41:1842–8.

36. Quarantelli M, Berkouk K, Prinster A, Landeau B, Svarer C, Balkay L, et al. Integrated software for the analysis of brain PET/SPECT studies with partial-volume-effect correction. J Nucl Med 2004;45:192–201.

37. Tzourio-Mazoyer N, Landeau B, Papathanassiou D, Crivello F, Etard O, Delcroix N, et al. Automated Anatomical Labeling of Activations in SPM Using a Macroscopic Anatomical Parcellation of the MNI MRI Single-Subject Brain. Neuroimage 2002;15:273–89.

38. Davatzikos C, Shen D, Gur RC, Wu X, Liu D, Fan Y, et al. Whole-brain morphometric study of schizophrenia revealing a spatially complex set of focal abnormalities.

Archives of General Psychiatry 2005;62:1218–27.

39. Magnin B, Mesrob L, Kinkingnéhun S, Pélégrini-Issac M, Colliot O, Sarazin M, et al. Support vector machine-based classification of Alzheimer's disease from whole-brain anatomical MRI. Neuroradiology 2009;51:73–83.

40. Chang CC, Lin CJ. LIBSVM: a library for support vector machines. ACM Transactions on Intelligent Systems and … 2011;

41. Chu C, Ni Y, Tan G, Saunders CJ, Ashburner J. Kernel regression for fMRI pattern prediction. Neuroimage 2011;56:662–73.

42. Rondina JM, Squarzoni P, Souza-Duran FL, Tamashiro-Duran JH, Scazufca M, Menezes PR, et al. Framingham Coronary Heart Disease Risk Score Can be Predicted from Structural Brain Images in Elderly Subjects. FrontiAgNeurosci 2014;6:300.

43. Byun H, Lee SW. Applications of support vector machines for pattern recognition: A survey. In: Lecture Notes in Computer Science. Pattern recognition with support vector machines; 2002. pages 213–36.

44. Fu WJ, Carroll RJ, Wang S. Estimating misclassification error with small samples via bootstrap cross-validation. Bioinformatics 2005;21:1979–86.

45. Rondina JM, Hahn T, de Oliveira L, Marquand AF, Dresler T, Leitner T, et al. SCoRS--A Method Based on Stability for Feature Selection and Mapping inNeuroimaging [corrected]. IEEE T Med Imaging 2014;33:85–98.

46. Kloppel S, Stonnington CM, Chu C, Draganski B, Scahill RI, Rohrer JD, et al. A plea for confidence intervals and consideration of generalizability in diagnostic studies. Brain 2008;132:e102–2.

47. Jack CR, Knopman DS, Jagust WJ, Shaw LM, Aisen PS, Weiner MW, et al. Hypothetical model of dynamic biomarkers of the Alzheimer's pathological cascade. The Lancet Neurology 2010;9:119–28.

48. Herholz K, Schopphoff H, Schmidt M, Mielke R, Eschner W, Scheidhauer K, et al. Direct comparison of spatially normalized PET and SPECT scans in Alzheimer's disease. J Nucl Med 2002;43:21–6.

49. Morinaga A, Ono K, Ikeda T, Ikeda Y, Shima K, Noguchi-Shinohara M, et al. A comparison of the diagnostic sensitivity of MRI, CBF-SPECT, FDG-PET and cerebrospinal fluid biomarkers for detecting Alzheimer's disease in a memory clinic. Dement Geriatr Cogn 2010;30:285–92.

50. Nihashi T, Yatsuya H, Hayasaka K, Kato R, Kawatsu S, Arahata Y, et al. Direct comparison study between FDG-PET and IMP-SPECT for diagnosing Alzheimer's disease using 3D-SSP analysis in the same patients. Radiat Med 2007;25:255–62.

51. Silverman DHS. Brain 18F-FDG PET in the diagnosis of neurodegenerative dementias: comparison with perfusion SPECT and with clinical evaluations lacking nuclear imaging. J Nucl Med 2004;45:594–607.

52. López MM, Ramírez J, Górriz JM, Alvarez I, Salas-Gonzalez D, Segovia F, et al. SVM-based CAD system for early detection of the Alzheimer's disease using kernel PCA and LDA. Neurosci Lett 2009;464:233–8.

53. Padilla P, Górriz JM, Ramírez J, Lang EW, Chaves R, Segovia F, et al. Analysis of SPECT brain images for the diagnosis of Alzheimer's disease based on NMF for feature extraction. Neurosci Lett 2010;479:192–6.

54. Yun HJ, Kwak K, Lee J-M, Alzheimer's Disease Neuroimaging Initiative. Multimodal Discrimination of Alzheimer's Disease Based on Regional Cortical Atrophy and Hypometabolism. PLoS ONE 2015;10:e0129250.

55. Duran FLS, Zampieri FG, Bottino CCM, Buchpiguel CA, Busatto GF. Voxel-based investigations of regional cerebral blood flow abnormalities in Alzheimer's disease using a single-detector SPECT system. Clinics 2007;62:377–84.

56. Lyketsos CG, Carrillo MC, Ryan JM, Khachaturian AS, Trzepacz P, Amatniek J, et al. Neuropsychiatric symptoms in Alzheimer's disease. 2011. pages 532–9.

57. Castro E, Gómez-Verdejo V, Martínez-Ramón M, Kiehl KA, Calhoun VD. A multiple kernel learning approach to perform classification of groups from complex-valued fMRI data analysis: application to schizophrenia. Neuroimage 2014;87:1–17.

58. Zhang D, Shen D, Alzheimer's Disease Neuroimaging Initiative. Predicting future clinical changes of MCI patients using longitudinal and multimodal biomarkers. PLoS ONE 2012;7:e33182.

59. Ardekani BA, Bermudez E, Mubeen AM, Bachman AH, Alzheimer's Disease Neuroimaging Initiative. Prediction of Incipient Alzheimer's Disease Dementia in Patients with Mild Cognitive Impairment. J Alzheimers Dis 2017;55:269–81.

60. Farzan A, Mashohor S, Ramli AR, Mahmud R. Boosting diagnosis accuracy of Alzheimer's disease using high dimensional recognition of longitudinal brain atrophy patterns. Behavioural Brain Research 2015;290:124–30.

61. Young J, Modat M, Cardoso MJ, Mendelson A, Cash D, Ourselin S, et al. Accurate multimodal probabilistic prediction of conversion to Alzheimer's disease in patients with mild cognitive impairment. Neuroimage Clin 2013;2:735–45.

62. Zhang D, Wang Y, Zhou L, Yuan H, Shen D, Alzheimer's Disease Neuroimaging Initiative. Multimodal classification of Alzheimer's disease and mild cognitive impairment. Neuroimage 2011;55:856–67.

63. Challis E, Hurley P, Serra L, Bozzali M, Oliver S, Cercignani M. Gaussian process

classification of Alzheimer's disease and mild cognitive impairment from resting-state fMRI. Neuroimage 2015;112:232–43.

64. Dyrba M, Ewers M, Wegrzyn M, Kilimann I, Plant C, Oswald A, et al. Robust automated detection of microstructural white matter degeneration in Alzheimer's disease using machine learning classification of multicenter DTI data. PLoS ONE 2013;8:e64925.

65. Zhang Y, Wang S, Phillips P, Yang J, Yuan T-F. Three-Dimensional Eigenbrain for the Detection of Subjects and Brain Regions Related with Alzheimer's Disease. J Alzheimers Dis 2016;50:1163–79.

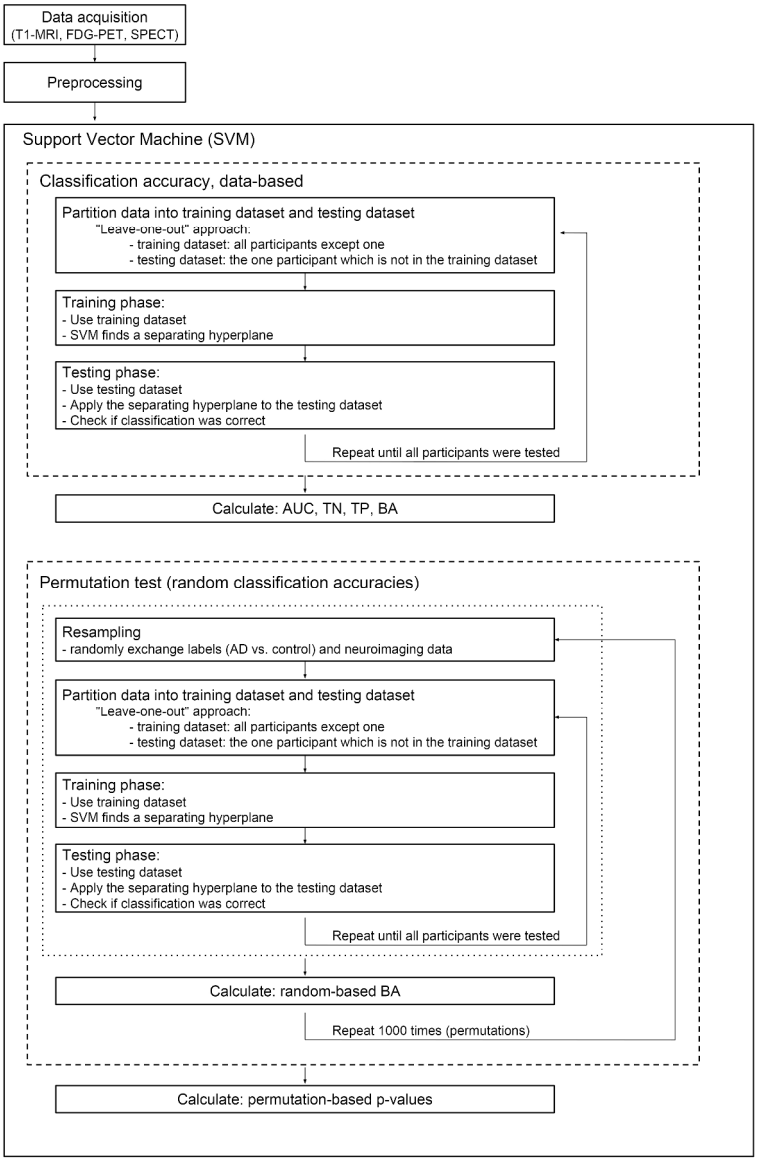

Figure 1. Flow chart of SVM analysis. Legend: AD: Alzheimer's disease; AUC, area under curve; BA: balanced accuracy; FDG-PET: 18F-fluorodeoxyglucose-positron emission tomography; SPECT: single photon emission computed tomography; SVM: support vector machine; T1-MRI: T1-weighted magnetic resonance imaging; TN: true negative TP: true positive.
Fig1_SVM_Flowchart.tif
305x453mm (300 x 300 DPI)

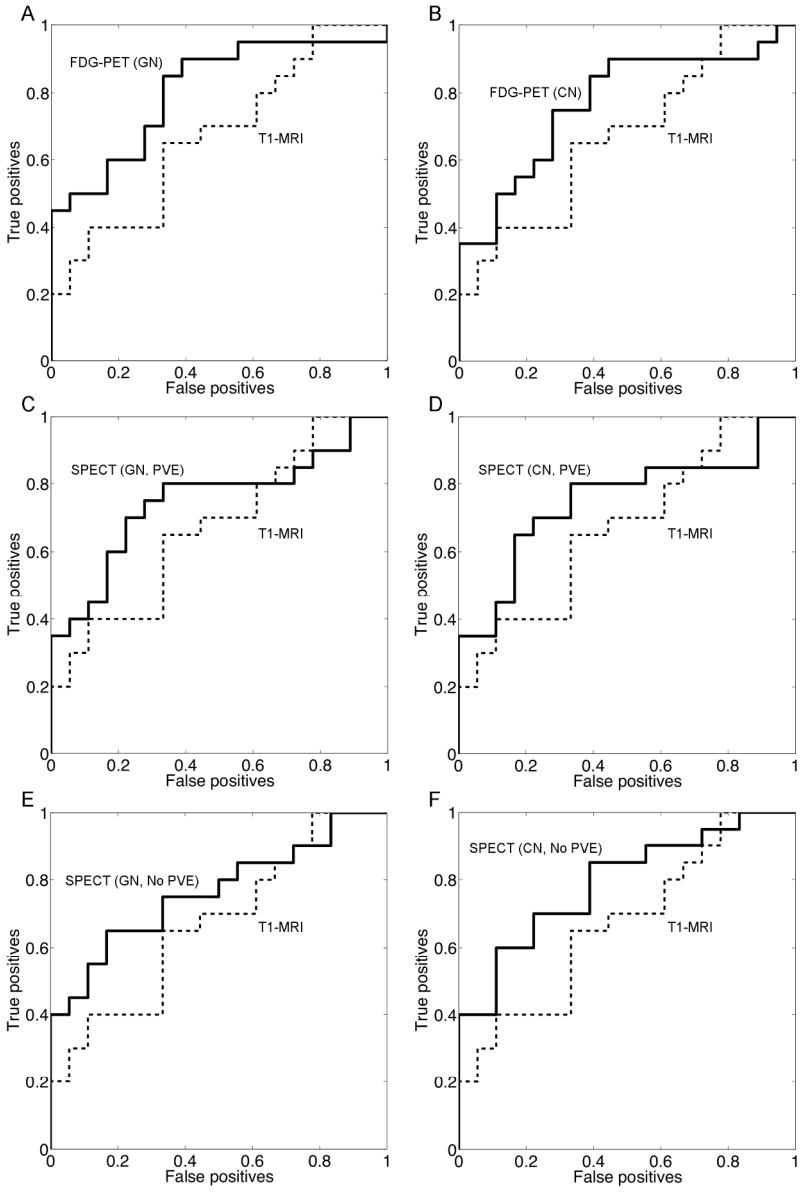

Figure 2. Receiver operating characteristic (ROC) curves of single modality classification. Legend: CN: cerebellar normalization; FDG-PET: 18F-fluorodeoxyglucose-positron emission tomography; GN: global normalization; PVE: partial volume effect correction; SPECT: single photon emission computed tomography; T1-MRI: T1-weighted magnetic resonance imaging.
Fig2_ROC_Single_Modalities.tif
173x246mm (300 x 300 DPI)

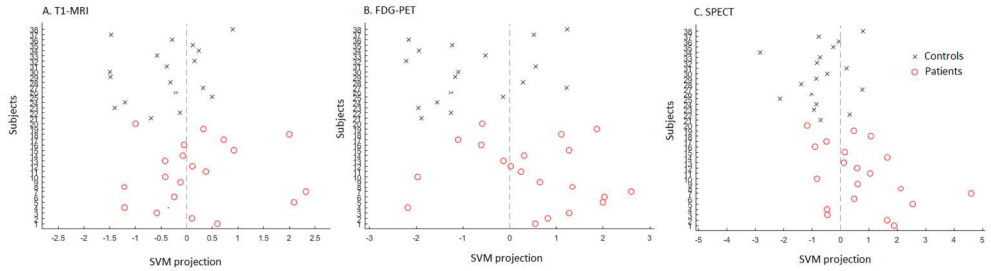

Figure 3. SVM class prediction of individual subjects for each imaging modality. Legend: Y-axis: subject's identification number. X-axis: linear projection of each subject. Subjects receiving negative values (i.e. data points to the left of the vertical dotted line) were classified as Controls while those receiving positive values (i.e. to the right of the vertical line) were classified as having Alzheimer's disease (AD). Misclassifications can be observed as circles at the left side of the separating plane (AD patients incorrectly classified as Controls, i.e. false negatives) and crosses at the right side of it (Controls incorrectly classified as AD patients, i.e. false positives). FDG-PET: 18F-fluorodeoxyglucose-positron emission tomography; SPECT: single photon emission computed tomography; SVM, support vector machine; T1-MRI: T1-weighted magnetic resonance imaging.
Fig3_Individual_Predictions.ti
438x124mm (96 x 96 DPI)

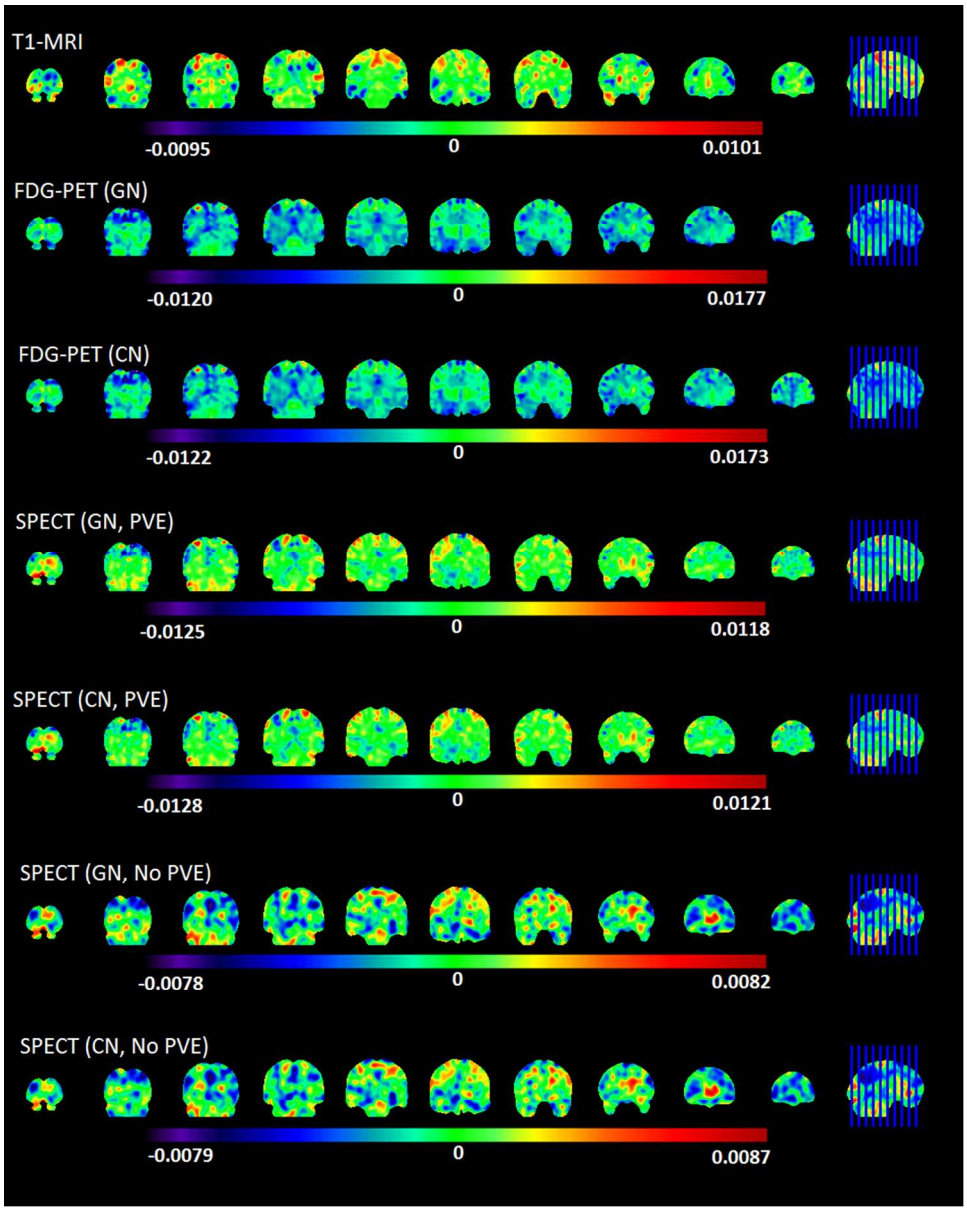

Figure 4. Patterns of anatomical distribution of voxel weights resulting from single-modality classifications. Legend: Positive weights mean a higher relative measure in that voxel for AD patients compared to Controls. Conversely, a negative weight means a higher relative measure for Controls. The measures are: grey matter volume for T1-MRI, regional brain metabolism for FDG-PET and regional cerebral blood flow for rCBF-SPECT. CN: cerebellar normalization; FDG-PET: 18F-fluorodeoxyglucose-positron emission tomography; GN: global normalization; PVE: partial volume effect correction; SPECT: single photon emission computed tomography; T1-MRI: T1-weighted magnetic resonance imaging.
Fig4_WeightMaps.tif
90x113mm (300 x 300 DPI)

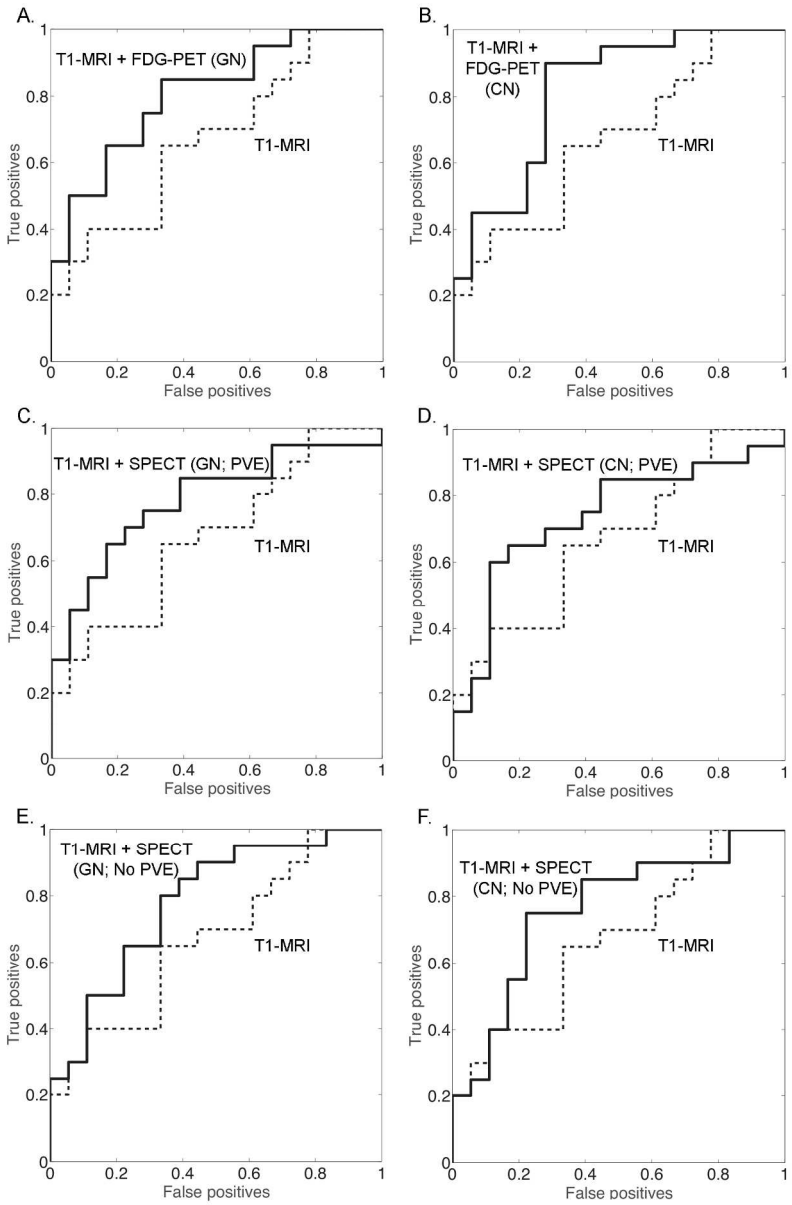

Figure 5. Receiver operating characteristic (ROC) curves of classifications using combination of imaging modalities. Legend: CN: cerebellar normalization; FDG-PET: 18F-fluorodeoxyglucose-positron emission tomography; GN: global normalization; PVE: partial volume effect correction; SPECT: single photon emission computed tomography; T1-MRI: T1-weighted magnetic resonance imaging.
Fig5_ROC_Combined_Modalities.t
173x250mm (300 x 300 DPI)